Coursework 4 - Magnetic Resonance Fingerprinting

University College London

Medical Physics & Biomedical Engineering department

MRes - Coursework 4

COMP0121 - Computational MRI

AUTUMN Term

18th April 2021

Author:
Mr. Imraj Singh (SN: 20164771)

Module lead:
Dr. Gary Zhang
Graduate Teaching Assistant:
Mr. Sean Epstein

This report will form the basis of the introduction of my MRes report. Some basic concept have been simulated and can be found in my GitHub repository

Contents

1 Multiparametric MRI

Magnetic resonance imaging (MRI) is a mature technology that is readily available for clinical use. This use is typically qualitative, where weighted images are evaluated with regards to hypointense and hyperintense regions. Over the past decade, there has been a strong interest in making these scans more quantitative. By making scanning more quantitative more information can be obtained, for example, the function not only structure could be evaluated. Quantification consist of maps of specific parameters of the tissue. These parameters are obtained through hand-crafted pulse sequences. The pulse sequences use radio frequency pulses, and magnetic field gradients, strengths and orientations, which are varied in time to interrogate a specific parameter of interest. These quantitative multiparametic maps give new insight into the progression, treatment and diagnosis of disease, enabling the development of novel biomarkers. An example of this is prostate cancer diagnosis [1], where multiparametric MRI is gaining clinical adoption as a standard of care for the diagnosis of prostate cancer. For increased clinical adoption, the acquisition time has to be decreased allowing higher patient throughput and patient comfort. Speeding up acquisition requires a divergence from classically defined pulse sequences.

2 Magnetic Resonance Fingerprinting

In 2013 a paper outlining a novel acquisition and reconstruction technique for quantitative multi-parametric MRI was published [2]. This was the seminal work on Magnetic Resonance Fingerprinting (MRF). The basic concept is by leveraging the underlying physics governing nuclear magnetisations a dictionary of signal evolutions over time can be created. This dictionary can be mapped, on a voxel-by-voxel basis, to the measured voxel signal evolution. Using simulations of the underlying physics to interpret the signal departs from traditional pulse-sequences which rely on steady-state magnetisation [3]. The signal acquisition is taken pseudo-randomly, with the original pulse-sequence [2] interrogating the parameters T_1, T_2 and off-resonance frequency. The acquisition includes read-out which is typically highly undersampled with various k-space trajectories to reduce acquisition time, variable density spiral in [2]. From Fig. 1 the pulse-sequence is given by both the temporal and spatial incoherence blocks. The temporal incoherence refers to the part of the pulse-sequence that interrogates specific parameters of interest. The spatial incoherence refers to the undersampling trajectory in k-space.

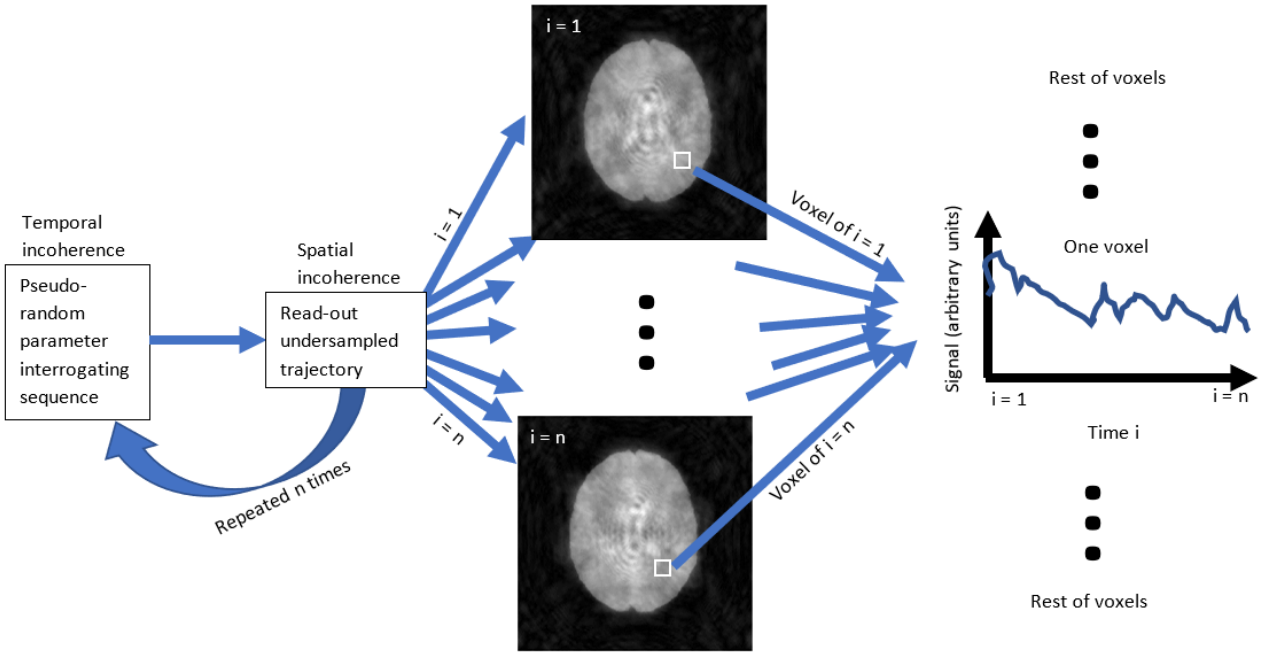

Figure 1: Basic diagrammatic representation of magnetic resonance fingerprinting, where the outputted voxel signal is mapped to the dictionary to obtain parameters of interest.

Each read-out is filtered back-projected into image space to find individual voxel signals. These voxel signals populate signal evolution graphs for each voxel, which are in-turn matched against simulations to obtain the tissue parameters of interest.

2.1 Acquisition

The novel approach to acquisition relies primarily on the notion of incoherence. This incoherence is produced spatially and temporally and allows the separation of underlying tissue parameters within reasonable acquisition times. More precisely, in the case of original inversion-recovery balanced steady state free-precession (IR-bSSFP) sequence [2], the flip angle (FA) of the radio frequency pulse and repetition time (RT) were varied pseudo-randomly to introduce temporal incoherence. The temporal incoherence has been extended to allow the quantification of other underlying tissue parameters such as T_2^* and various micro-structure parameters [4]. The pulse-sequence parameters (i.e. FA and RT from [2]) can be chosen and set such that specific underlying tissue parameters of interest will be promoted. This can be seen as the "Pseudo-random parameter interrogating sequence" in Fig. 1. The optimally of temporal incoherence, and the clinical significance of the underlying tissue parameters which are promoted is outside of this report. The recent review [4] provides further reading.

2.2 Undersampling

Spatial incoherence is introduced due to the need to undersample k-space to ensure timely acquisition.

Signals are obtained directly in k-space. Traditionally, the Shannon-Nyquist sampling theorem specified the amount of samples that should be taken in k-space to exactly reconstruct the image. This sampling procedure was done line-by-line in k-space. This ensured that every value of k-space represented a new phase over the imaging domain, and that the same number of points are sampled in k-space than the voxels that are reconstructed. This full-sampling technique requires long acquisition times and are not necessary for MRF.

Within biological images the k-space representation does not require all k-space to be sampled as the majority of information content is held at the center of k-space (low spatial frequency components). Thus trajectories that undersample k-space were developed. These included radial, Cartesian, and spiral k-space trajectories. Through undersampling, the system of mapping k-space measurements to the image becomes under-determined, and although parallel imaging is often employed which acquires more measurements aiding with reconstruction, artifacts are still produced when images are reconstructed through filtered back-projection. This is explored in the following figures. A horizontal slice of a brain is forward projected into k-space in Fig. 2, this k-space is used to test various undersampling trajectories.

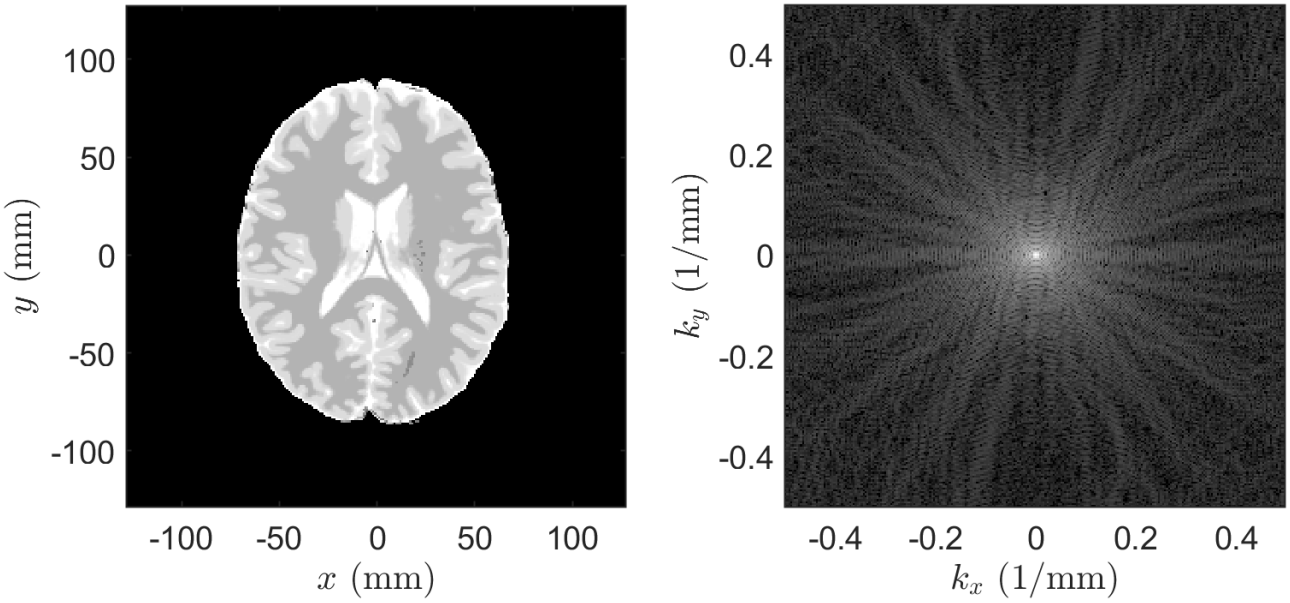

Figure 2: Full k-space representation of brain image. Logarithmic scale used for k-space and the absolute value of the signal is taken.

The effect of Cartesian undersampling is shown in Fig. 3, where only every tenth row of k-space was kept. This resulted in only 10% of the original signal being kept. This percentage of undersampling (10%) was kept constant for all proceeding undersampling trajectories presented (Cartesian, radial, spiral and golden angle radial). It is observed that there is aliasing with the image repeating itself producing a coherent patterned in the vertical direction. By missing rows in k-space the phase-encoding direction is undersampled. Therefore the field of view in the phase-encoding direction changes such that the position wraps to the opposite side of the image. This wrapping is a feature of the frequency representation of the image where the field of view in the phase-encoding direction is effectively changed through undersampling.

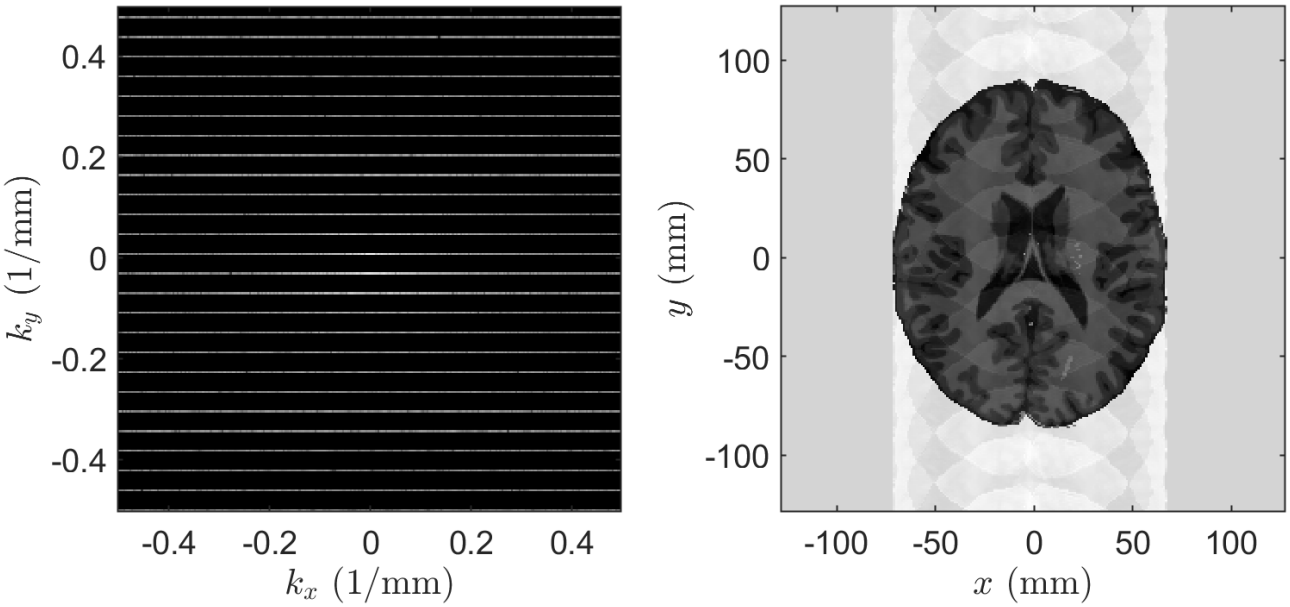

Figure 3: Cartesian undersampling. Logarithmic scale used for k-space and the absolute value of the signal is taken.

A radial undersampling k-space trajectory can be seen in Fig. 4. When compared with the Cartesian undersampling there is a much less coherent structure to the artifacts that are obtained.

Looking closely, it can be noted that there are fringing artifacts that appear tangent to the central image structure (the brain) this is typical of radial undersampling. The Cartesian trajectory is able to capture nuances in the images much better than the radial undersampling. This can be attributed to Cartesian undersampling sampling fully along rows, thus providing high fidelity image information with regards high spatial frequency components which contribute more to the nuances of the image. The radial sampling does capture more of the center of k-space and the overall structure is better with voxel values being more in-line with Fig. 2, i.e. the brain is shown as white rather than black in Fig. 3.

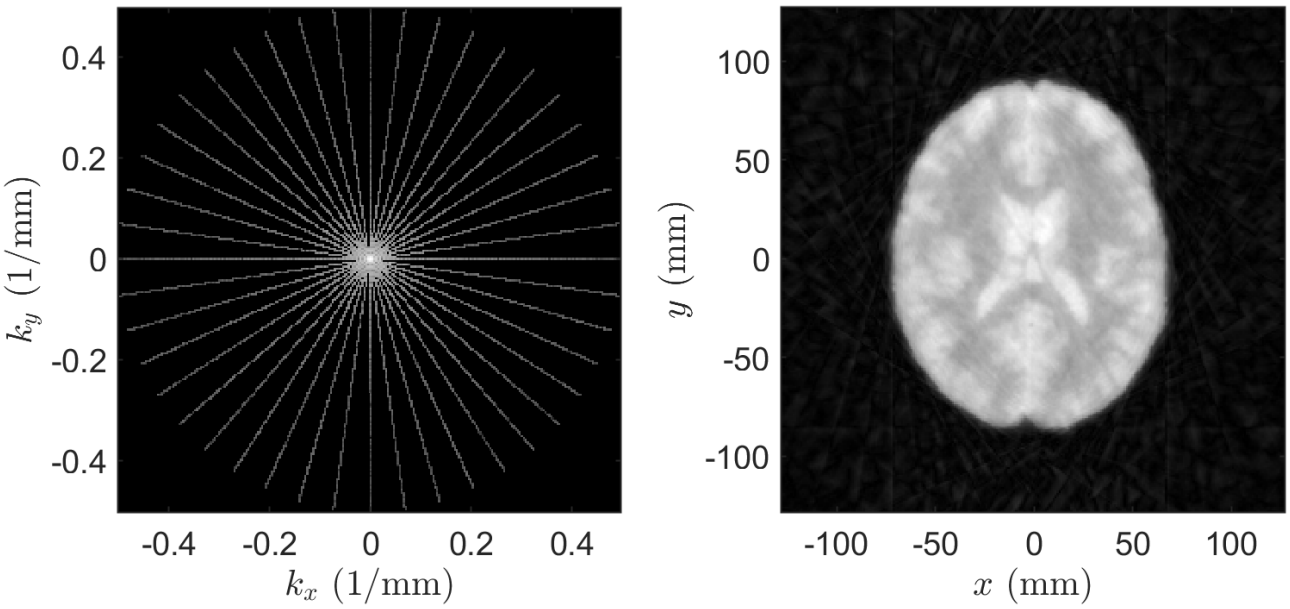

Figure 4: Radial undersampling. Logarithmic scale used for k-space and the absolute value of the signal is taken.

A spiral trajectory was simulated. From Fig. 5 it can be seen that, again, the overall structure of the image is maintained. Instead of a tangential fringe artifact there are ringing artifacts. The nuances of the image are dominated by the ringing artifacts.

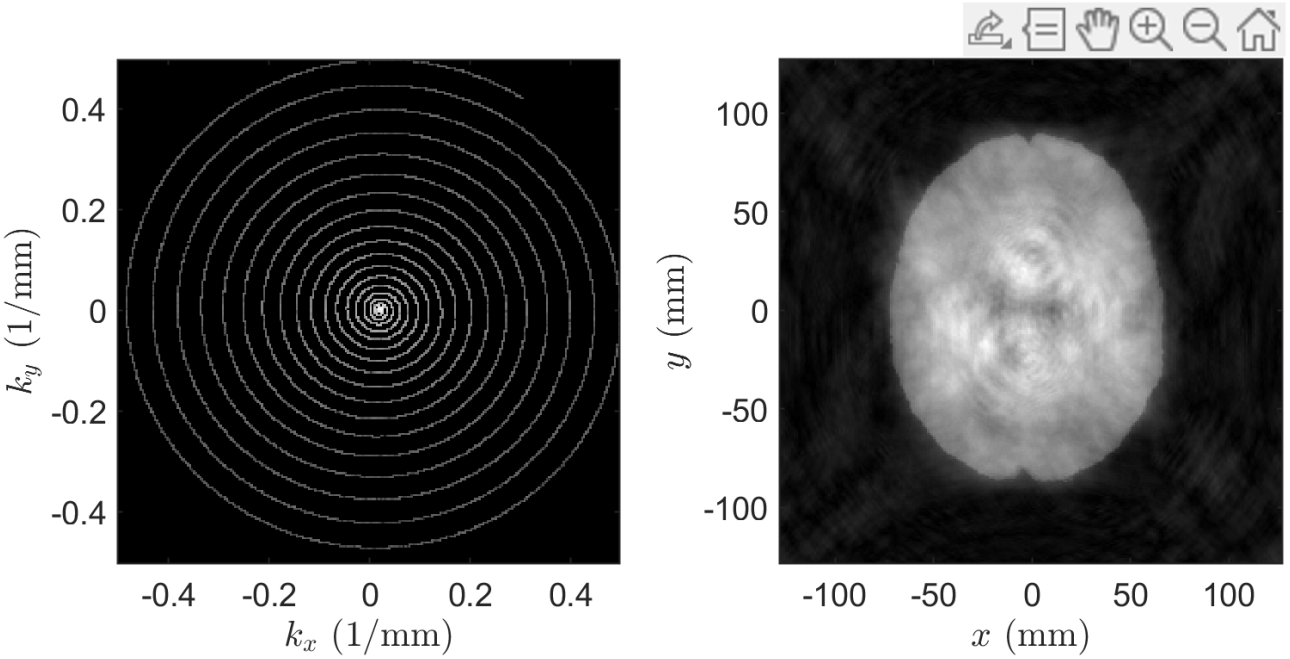

Figure 5: Spiral undersampling. Logarithmic scale used for k-space and the absolute value of the signal is taken.

Finally in Fig. 6, a golden angle radial undersampling is assessed. The golden angle undersampling is such that each radial line is incline at the angle of the previous radial line plus the golden angle. Using this golden angle "step" ensures that any one radial line will never overlap another radial line. When this undersampling trajectory is used it has been shown to give more incoherent artifact [5]. Unfortunately, from comparison of Fig. 6 against Fig. 4, incoherence is not observed but instead the tangential fringing artifact is seen. This is most likely due to the fact these undersampling trajectories are created through masking values of forward projected brain image k-space, see Fig. 1. Through defining the undersampled k-space by nearest neighbour of the undersampling trajectories and the k-space which is a 256x256 uniform grid, we introduce error into the trajectories. This is seen on all undersampled figures as the trajectories appear pixelated. The k-space should instead be sampled at the points exactly corresponding to the trajectory and then re-gridded back onto a regular grid so that this can be filtered back-projected via the discrete inverse Fourier transform to obtain the undersampled image. This requires a re-gridding algorithm for k-space. There are several gridding algorithms which are outlined in [6]. For this report these are not implemented.

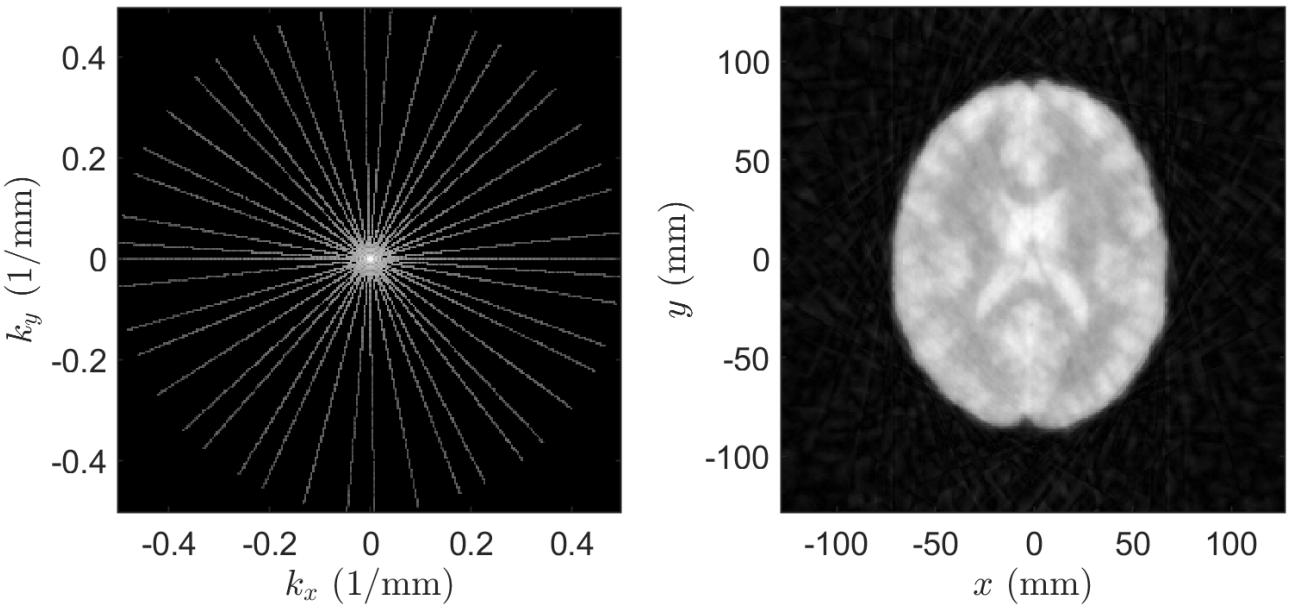

Figure 6: Golden-angle radial undersampling. Logarithmic scale used for k-space and the absolute value of the signal is taken.

A relatively new technique that has been leveraged for exactly reconstructing undersampled signal is compressed sensing. In compressed sensing the aim is to design a undersampling strategy together with a mutually incoherent image representation such that images can be robustly reconstructed under an appropriate sparsity constraint and its corresponding proximal operator (e.g. soft thresholding). As demonstrated by Figs, 3, 4, 5 and 6, the undersampling trajectories produce coherent artifacts which do not satisfy the mutual incoherence criterion, thus limiting the success of compressed sensing methods. Undersampling trajectories that satisfy the mutual incoherence criterion are of interest, and this was a motivation in the development of golden angle radial sampling trajectory. Recent research has shown that machine learning reconstruction techniques have been successfully leveraged to reconstruct images with coherent artifacts. Machine learning additional has the ability to greatly speeding up reconstruction times [5].

Deriving these undersampling trajectories is a nontrivial task, recent work [7] utilises deep learning techniques to define sampling patterns. This work omitted the measurement constraints defined by the scanner. It is important to include an assessment of physical plausibility when assessing undersampling trajectories. An outline of how to define physically plausible trajectories from proposed sampling patterns is given in [8].

Along with the physical constraints of the scanner it is important to take into account the comfort of the patient. Sharply changing read-out gradients are experienced as loud and disconcerting noises. These noises can increase patient anxiety, and my induce unwanted movement, particularly in sensitive patient populations. Freedom in the read-out of MRF can be used to instead of creating dissonance, create music. This was demonstrated in [9].

The constraints of undersampling trajectories for MRF are: spatial incoherence such that coherent artifacts are minimised; resolution obtained through each read-out should be maximised; the time for read-out should be minimised; that the trajectories are physically plausible given scanner constraints; and noise should be minimised to increase patient comfort.

Signal is acquired directly into k-space, where each point in k-space represents the whole image domain. To find a voxel signal, the obtained k-space signal must be reconstructed into an image, in Fig. 1 for reconstruction occurs from read-out to image $i = 1$ to $i = n$. In MRF this is typically direct inversion through the adjoint operator, i.e. discrete inverse Fourier transform - filtered back-projection. This is the reconstruction method used in [2].

2.3 Dictionary

The dictionaries to which the voxel signal evolutions are matched are produced through simulation. These simulations can include varying degrees of dynamics. The most basic is simulation of a single nuclear magnetisation through the Bloch equation:

$$\frac{d\overrightarrow{M}}{dt} = \gamma\overrightarrow{M} \times \overrightarrow{B}_{ext} + \frac{1}{T_1}(M_0 - M_z)\hat{z} - \frac{1}{T_2}\overrightarrow{M}_{\perp} \tag{1}$$

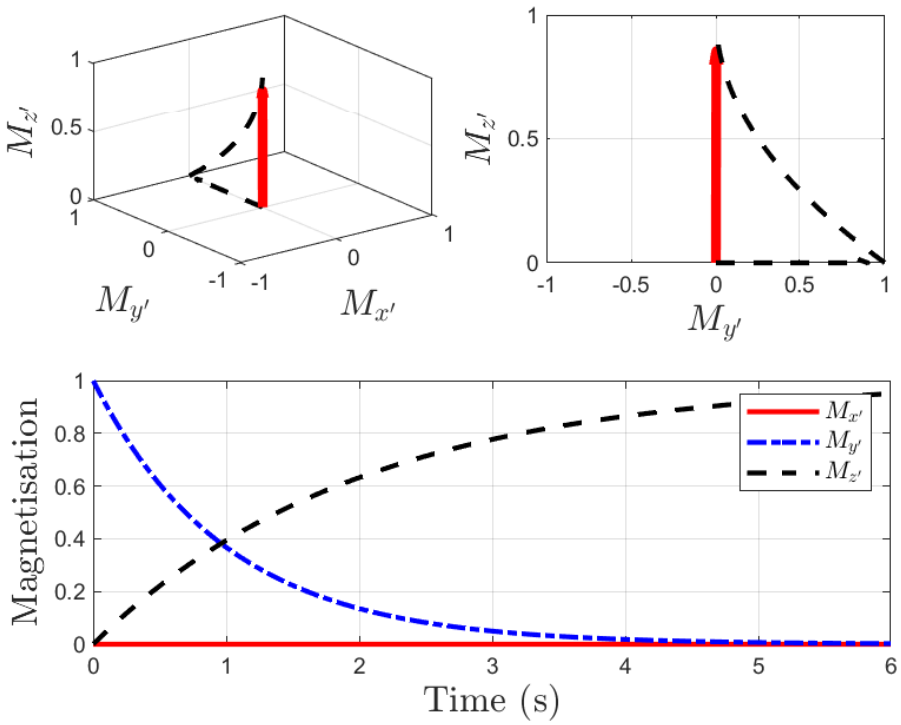

Figure 7: Exponential decay from of a single isochromat in a rotating frame of reference. Top left give the magnetisation vector trajectory in 3D space, top right, gives the trajectory in 2D space, and bottom gives the evolution of the different components of the magnetisation vector. This is all in the rotating frame of reference. $T_1 = 1$ and $T_1 = 2$

Eqn. 1 is set of ordinary differential equations; where $\overrightarrow{M}$ is a vector of magnetisations in the x,y,z directions, $\overrightarrow{B}$ is the external magnetic field, M_0 is the initial magnetic vector magnitude, and $\overrightarrow{M}_\perp$ is the transverse magnetisation which produces the signal. The solution of this equation is known, and has two characteristics, an exponential decay in both transverse and longitudinal directions, and a rotation. As can be seen in Fig. 7, by using a frame of reference which is coincident with the Larmor frequency of the isochromat, the high frequency rotations are halted, i.e. only the exponential decay is observed. The dynamics that can be captured through this simulation are T_1, T_2 and M_0. This formulation does not take into account diffusion dynamics. Including this dynamic gives the Bloch-Torrey equation:

$$\frac{d\overrightarrow{M}}{dt} = \gamma\overrightarrow{M} \times \overrightarrow{B}_{ext} + \frac{1}{T_1}(M_0 - M_z)\hat{z} - \frac{1}{T_2}\overrightarrow{M}_\perp + \Delta \cdot \overrightarrow{D}\Delta\overrightarrow{M} \tag{2}$$

The solution of Eqn. 2, is the same as for Eqn. 1, but with the addition of diffusion there is added exponential decay. It should be noted that the diffusion tensor $\overrightarrow{D}$ is an identity matrix in the case of isotropic diffusion, and that diffusion weighted imaging requires diffusion probing gradients, which increase scan time. This quite simply demonstrates that if dynamics are ignored then this can result from a divergence from reality if the ignored dynamics contribute to signal substantially. This is commonly referred to as model error. It is important to include as much of the underlying dynamics into simulations as possible.

To obtain a more realistic magnetisation response an array of isochromats with a variety of off-resonance frequencies need to be simulated. For large quantities of isochromats this becomes computationally expensive to compute dictionaries of voxel signal evolutions. Instead of the off-resonance of the isochromats consider them as at different points in a spatially varying magnetic field. This interpretation has the effect being able to interpret the off-resonance as signal contributions to specifc Fourier basis', as applying gradients to spatially distributed isochromats allows the signal of specific spatial frequencies to be sampled.

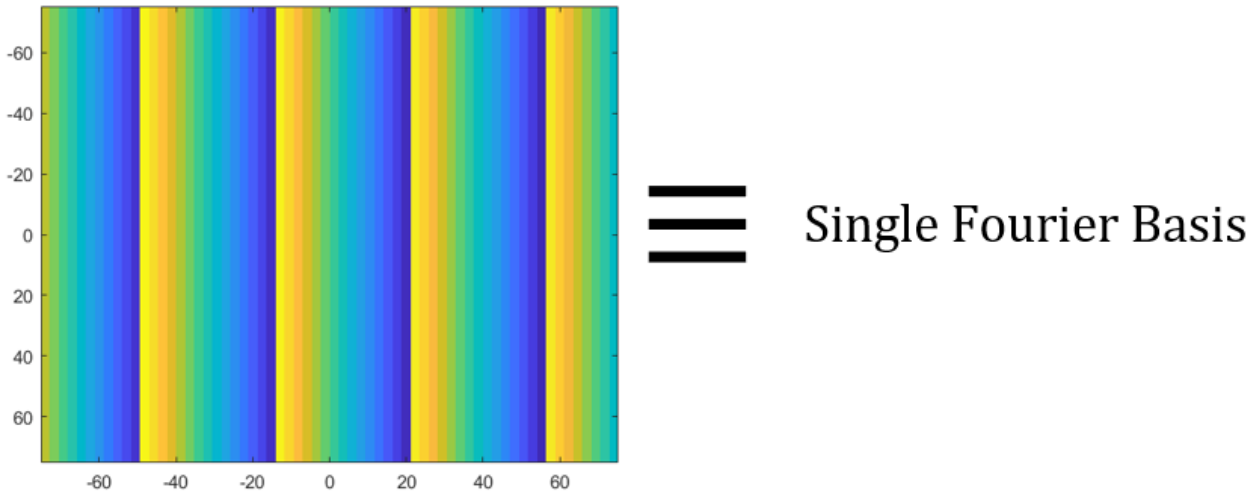

Figure 8: (left) an array of identical isochromats uniformly distributed in a grid after action of a dephasing gradient over some time. The axes give the spatial location, and colour gives the phase of the isochromats. (right) giving the equivalence to the magnitude of a single Fourier basis.

Making an equivalence between the evolution of an array of isochromats with different off-resonance frequencies as the magnitude of specific Fourier basis' gives an understanding of the motivation of Extended Phase Graphs (EPG) [10]. EPG treats the evolution of an array of isochromats with different off-resonance frequencies solely in the Fourier domain, this greatly simplifies the computation. Furthermore, dynamics such as diffusion, coherent motion and the relaxation can all be captured by EPG. EPG will be explored as the method to simulate the signals.

Once a dictionary of signals is captured, they are matched to the measured signal on a voxel-by-voxel basis. In [2] this was done through an exhaustive search whilst minimising the residual between the measured voxel signal evolution and the simulation. This was computationally expensive and lead to long reconstruction times. More recent work [3, 11, 12] leverages low-rank iterative methods (often leveraging singular value decomposition) to speed up reconstruction. It can be noted that the reduction in acquisition time is typically at the expense of reconstruction time.

3 Avenues of work

Research into speeding up and increasing accuracy of reconstruction has been focused on a basic projection into the image domain followed by dictionary matching. A different perspective that will be explored is exploiting the spatial incoherence and multitude of poorly reconstructed images to inform one-another to obtain more accurate projections into image space. These more accurate projections could improve voxel-by-voxel matching to the simulated signal evolutions.

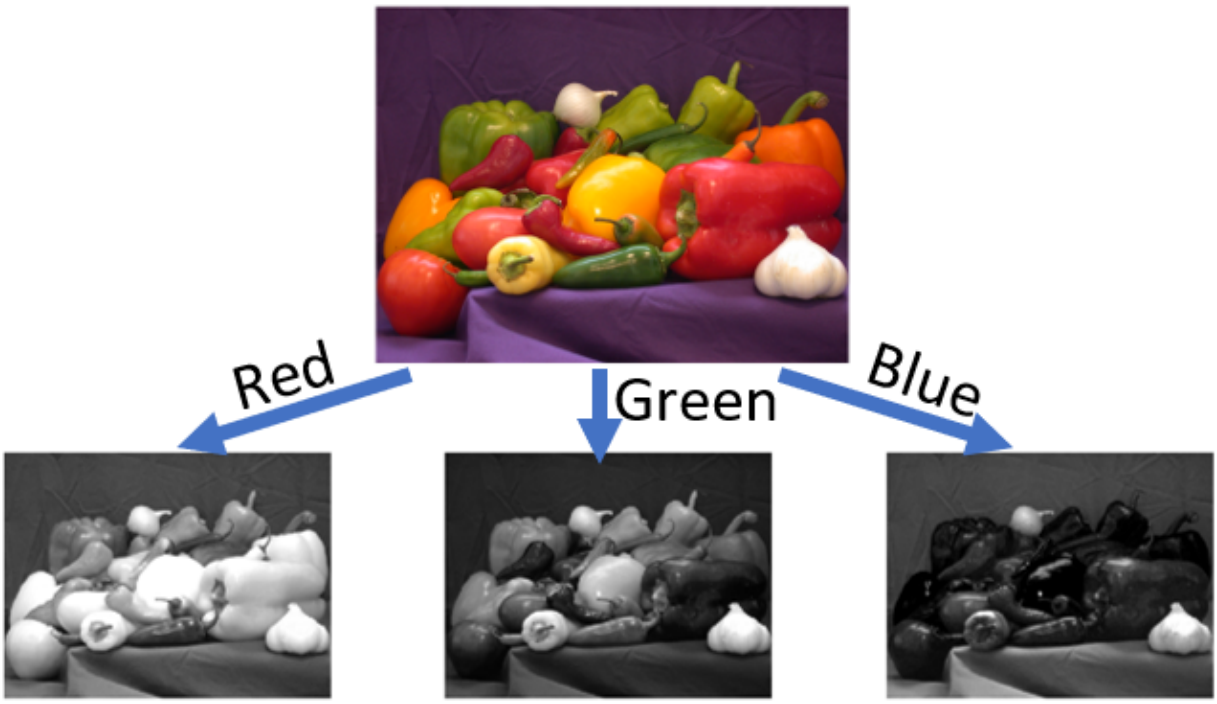

Figure 9: An image can be split into multiple channels, for example red, green and blue. The underlying structure of image is present in the channels.

Fig. 9 demonstrates that a colour image can be split into the underlying channels, i.e. red, green and blue. These channels share common structure as they describe the same components of the underlying image. A parallelism can be made with the poorly reconstructed images, where they can be thought of as different channels of the same underlying tissue image. More explicitly, there is a common structure in the poorly reconstructed images that corresponds to the different tissues present and these different tissues have different parameter values, i.e. T_1 and T_2. Through the pulse sequence these parameters are promoted such that the tissues are separable, such that even poorly reconstructed images exhibit promoted parameters. Sharing information between poorly reconstructed images could promote underlying structure to be expressed, and could provide improved reconstruction of the individual channels. This could lead to more accurate matching and assessment of tissue parameters. Furthermore, acquisition could be accelerated further as fewer temporal points of the signal would potentially need to be captured. This is because by sharing information between channels the voxel signals could be more accurately determined.

Conceptually, each read-out in MRF corresponds to an image with a small amount of information. MRF typically has between 500-3000 read-outs [13]. As proposed, by sharing information between read-outs ("channels"), the underlying structural information of the read-outs can be promoted. After reasonable reconstructions are obtained, through sharing structural information, matching algorithms can be used to obtain the quantitative multiparametric maps. The divergence from typical MRF is that information is shared not only implicitly at the matching stage, but it is also shared when the read-out is projected in to image domain. By sharing information at this earlier stage it may reduce the number of read-outs required as well as improving matching accuracy to simulations.

The concept of sharing information across channels is the basis of joint reconstruction. Typically, joint reconstruction is done with only a few channels and is used to promote common structural features across the channels. This can be done through the prior in the iterative reconstruction framework. These priors include joint/vectorial total variation, parallel level sets, and joint entropy methods [14]. These methods can penalise parts of the image based on the underlying structures of what is common among the channels. For example, if there are shared gradients (i.e. edges) across the channels we can promotes these gradients whilst penalising where these gradients are not shared. This is the basis of joint total variation regularisation.

There is an import factor to take into account with joint reconstruction. Coherent artifacts are often produced through undersampling trajectories. Careful attention must be taken in order to not promote these artifacts in the image. Additionally, undersampling trajectories should determined which produce incoherent artifacts. In [2] a variable density spiral was used for the undersampling trajectory. This trajectory was rotated by 90° between for each readout. This effectively increased spatial incoherence. It could be interesting to use a golden angle to rotate the trajectory to further increase the spatial incoherence. Instead of using all read-outs to promote the underlying structure of the image, only using the temporal "nearest neighbours" could be used. This could reduce computational load as well as still providing improvements to the reconstruction.

Finally, deep learning could be leveraged as it allows for powerful prior representation. Using a deep convolutional neural network for de-noising and de-aliasing was shown in [5]. De-noising and de-aliasing is essentially what is needed to make the individual read-outs more accurate. In addition to de-noising and de-aliasing, deep learning can be leveraged in the matching process [13]. An end-to-end method could be developed that takes information of the pulse sequence and the read-outs to produce the quantitative multiparametric maps, although this would require extensive training.

4 Conclusion

A brief review of MRF is given, with a focus on reconstruction. It is posited that sharing information between read-outs could improve reconstruction accuracy, and lower acquisition times further. The burden essentially moves from acquisition to reconstruction. The importance of undersampling trajectory is highlighted, and spatial incoherence will need to be explored to ensure that joint reconstructed methods do not promote coherent artifacts.

References

[1] A. Stabile, F. Giganti, A.B. Rosenkrantz, S.S. Taneja, G. Villeirs, I.S. Gill, C. Allen, M. Emberton, C.M. Moore, and V. Kasivisvanathan. Multiparametric MRI for prostate cancer diagnosis: current status and future directions. *Nature Reviews Urology*, 17(1):41–61, July 2019.

[2] D. Ma, V. Gulani, N. Seiberlich, K. Liu, J.L. Sunshine, J.L. Duerk, and M.A. Griswold. Magnetic resonance fingerprinting. *Nature*, 495(7440):187–192, Mar 2013.

[3] J. Assländer, M.A. Cloos, F. Knoll, D.K. Sodickson, J. Hennig, and R. Lattanzi. Low rank alternating direction method of multipliers reconstruction for mr fingerprinting. *Magnetic Resonance in Medicine*, 79(1):83–96, Mar 2017.

[4] B.B. Mehta, S Coppo, D.F. McGivney, J.I. Hamilton, Y. Chen, Y. Jiang, D. Ma, N. Seiberlich, V. Gulani, and M.A. Griswold. Magnetic resonance fingerprinting: a technical review. *Magnetic resonance in medicine*, 81(1):25—46, January 2019.

[5] A. Hauptmann, S. Arridge, F. Lucka, V. Muthurangu, and J.A. Steeden. Real-time cardiovascular mr with spatio-temporal artifact suppression using deep learning–proof of concept in congenital heart disease. *Magnetic Resonance in Medicine*, 81(2):1143–1156, Sep 2018.

[6] John Pauly. Non-cartesian reconstruction. Oct 2005.

[7] F. Sherry, M. Benning, J. C. De los Reyes, M. J. Graves, G. Maierhofer, G. Williams, C.B. Schönlieb, and M. J. Ehrhardt. Learning the sampling pattern for mri. *IEEE Transactions on Medical Imaging*, 39(12):4310–4321, 2020.

[8] C. Boyer, N. Chauffert, P. Ciuciu, J. Kahn, and P. Weiss. On the generation of sampling schemes for Magnetic Resonance Imaging. *SIAM Journal on Imaging Sciences*, 9(4):2039–20972, December 2016.

[9] D. Ma, E.Y. Pierre, Y. Jiang, M.D. Schluchter, K. Setsompop, V. Gulani, and M.A. Griswold. Music-based magnetic resonance fingerprinting to improve patient comfort during mri examinations. *Magnetic resonance in medicine*, 75(6):2303–2314, Jun 2016. 26178439[pmid].

[10] M. Weigel. Extended phase graphs: Dephasing, RF pulses, and echoes - pure and simple. *Journal of Magnetic Resonance Imaging*, 41(2):266–295, April 2014.

[11] G.L. da Cruz, A. Bustin, O. Jaubert, T. Schneider, R.M. Botnar, and C. Prieto. Sparsity and locally low rank regularization for MR fingerprinting. *Magnetic Resonance in Medicine*, February 2019.

[12] C.C. Cline, X. Chen, B. Mailhe, Q. Wang, J. Pfeuffer, M. Nittka, M.A. Griswold, P. Speier, and M.S. Nadar. AIR-MRF: Accelerated iterative reconstruction for magnetic resonance fingerprinting. *Magnetic Resonance Imaging*, 41:29–40, September 2017.

[13] D.F. McGivney, R. Boyacıoğlu, Y. Jiang, M.E. Poorman, N. Seiberlich, V. Gulani, K.E. Keenan, M.A. Griswold, and D. Ma. Magnetic resonance fingerprinting review part 2: Technique and directions. *Journal of Magnetic Resonance Imaging*, 51(4):993–1007, July 2019.

[14] M.J. Ehrhardt. Multi-modality imaging with structure-promoting regularisers, 2020.

A Scripts for Figures

Full scripts can be found on Github: https://github.com/Imraj-Singh/COMP0121.